Effective mass, spin fluctuations, and zero sound in liquid ^{3}He

H. R. Glyde
Department of Physics and Astronomy, University of Delaware, Newark, Delaware 19716

B. Fåk
Commissariat à l'Energie Atomique, Département de Recherche Fondamentale sur la Matière Condensée, SPSMS/MDN, 38054 Grenoble, France

N. H. van Dijk
Commissariat à l'Energie Atomique, Département de Recherche Fondamentale sur la Matière Condensée, SPSMS/MDN, 38054 Grenoble, France
and Delft University of Technology, Interfaculty Reactor Institute, 2629 JB Delft, The Netherlands

H. Godfrin
Centre de Recherches sur les Très Basses Températures, CNRS, Boîte Postale 166, 38042 Grenoble, France

K. Guckelsberger and R. Scherm
Physikalisch-Technische Bundesanstalt, Q1, D-38023 Braunschweig, Germany
(Received 17 May 1999)

We have measured and calculated the density and spin-density dynamic structure factors $S_c(Q,\omega)$ and $S_I(Q,\omega)$ of normal liquid ^{3}He as a function of wave vector Q and temperature T. The static spin susceptibility $\chi(T)$ and specific heat $C_V(T)$ are also calculated. These properties all depend upon the effective mass $m^*(k,\omega)$ of the Fermi quasiparticles making up the liquid. We use a model in which m^* peaks near the Fermi surface to $m^*=2.8$, the Landau theory effective mass, and decreases toward the bare mass $m^*=1$ for quasiparticles away from the Fermi energy ϵ_F. The theory for all the properties may be viewed as Landau theory with an effective mass $m^*(\epsilon_k)=m^*(k)$ that decreases as the quasiparticle energy ϵ_k moves away from ϵ_F. The peaking of m^* at ϵ_F is widely predicted in Fermi systems and the aim is to test how important this physical feature is in the dynamics of liquid ^{3}He. We find that $S_c(Q,\omega)$ and $S_I(Q,\omega)$ versus Q and T as well as $\chi(T)$ are well reproduced by the model for the same $m^*(k)$. The $C_V(T)$ can be reproduced, but a much lower value of $m^*(k)$ at energies ϵ_k away from ϵ_F is required, $m^*\simeq 0.5$, as found in previous calculations of $C_V(T)$. We conclude that the peaking of m^* at ϵ_F is an important physical feature to include in calculations of $S(Q,\omega)$ and that the quasiparticle model itself is inadequate for C_V at higher temperatures.

I. INTRODUCTION

A universal property of Fermi liquids is the enhancement of the quasiparticle effective mass m^* at or near the Fermi surface. This enhancement is found in nuclear matter, finite nuclei, liquid ^{3}He, liquid spin-polarized deuterium, and other exotic Fermi liquids. It was first noted by Brown *et al.*[1] and has been extensively documented and discussed in nuclei and liquid ^{3}He by Mahaux *et al.*[2] The aim of the present paper is to explore how well a simple model containing this enhancement of m^* can describe the spin fluctuations and zero sound observed in the dynamic structure factor $S(Q,\omega)$ of liquid ^{3}He. We also evaluate the dependence on temperature T of the specific heat $C_V(T)$ and the static spin susceptibility $\chi(T)$ with the same model. New neutron-scattering measurements of $S(Q,\omega)$ are presented for two different temperatures.

Fermi liquids may be described as a collection of Fermi quasiparticles moving in a self-consistent field arising from the other fermions. Much of the interaction between the bare Fermi particles can be incorporated into this self-consistent field. The field is represented by assigning an effective mass m^* to the particles and calling them quasiparticles. The remaining interaction between the quasiparticles is relatively small. This quasiparticle picture is the basis of the shell model of nuclei[2–4] and of Landau's Fermi liquid theory.[5,6] The resulting effective mass depends on the particle wave vector k and energy ω (we use energy units for ω in this paper), $m^*=m^*(k,\omega)$.[2,5] Physically, since the response functions of the fluid depend on wave vector and energy, the self-consistent field seen by the quasiparticle in the fluid and its resulting effective mass $m^*(k,\omega)$ depends on the quasiparticle momentum k and energy ω. Microscopic calculations[2,7–13] find that $m^*(k,\omega)$ peaks near $k=k_F$ or equivalently near $\omega=\epsilon_F$ (k_F and ϵ_F are the Fermi wave vector and energy, respectively). The quasiparticle effective mass is largest for quasiparticles on the Fermi surface. As k (or ω) moves away from k_F (or ϵ_F), m^* becomes smaller until it reduces to the bare mass m for $k\gg k_F$ or $\omega\gg\epsilon_F$. When the energy variable ω in m^* is restricted to the single-particle energy $\epsilon(k)$ [$\omega=\epsilon(k)$ only], $m^*(k,\omega)$ becomes a function of k only, $m^*(k,\epsilon(k))\equiv m^*(k)$.

The origin of the effective mass enhancement is the interaction between particles via the cooperative excitations in the fluid, the density, and spin-density fluctuations. Tradi-

tionally, spin fluctuations have been regarded[14–18] as the chief origin of m^*. In liquid ^{3}He and liquid deuterium, microscopic calculations[11–13] of $m^*(k,\omega)$ suggest that spin-density and density fluctuations contribute approximately equally to enhancing m^*. For example, in fully spin-polarized Fermi systems, where the fixed spin polarization prevents spin fluctuations, the enhancement of m^* is smaller but significant.[12,13] As the quasiparticle energy increases above ϵ_F and becomes high, much higher than the cooperative excitation energy, the excitations cannot respond to the quasiparticle motion[2,15,16] and $m^*(k,\omega)$ reduces to m.

At low temperatures, $k_BT \ll \epsilon_F$, quasiparticles are thermally excited from states just below ϵ_F to states just above ϵ_F, all within k_BT of the Fermi surface. Thus in thermal properties at low T, the effective mass of the participating quasiparticles will be $m^*(\epsilon_F)$. In liquid ^{3}He, for example, the Landau effective mass m^* appearing in Landau theory[6] obtained from C_V at $T \to 0$ is $m^* = m^*(\epsilon_F) = 2.8m_3$.[19,20] As T is increased quasiparticles away from ϵ_F having a smaller effective mass are excited. Thus the aggregate effective mass of the quasiparticles involved will be smaller as T increases. For example, the observed specific heat[19] has an abrupt reduction in slope at $T \simeq 0.25$ K as if the aggregate effective mass decreases quite rapidly at this temperature as quasiparticles further from ϵ_F are excited with increasing temperature. A complete description of $C_V(T)$ in Fermi liquids is very complicated,[16,21–24] but at higher temperatures, $k_BT \sim \epsilon_F/3$, the peaking of $m^*(k)$ at k_F is certainly a contributing factor in the apparent drop in the effective mass in $C_V(T)$. We explore this point in Sec. V where C_V is evaluated as a test of the present model.

Similarly, in neutron scattering experiments[25–30] quasiparticles are excited from states $\mathbf{k}$ ($k < k_F$) to states $\mathbf{k}+\mathbf{Q}$ ($|\mathbf{k}+\mathbf{Q}| > k_F$), where $\mathbf{Q}$ is the wave vector transfer from the neutron to the fluid. At low Q, only states immediately below k_F and immediately above k_F will be sampled and the quasiparticles involved will have a mass $m^*(k_F)$. As Q increases, quasiparticles further away from k_F are excited and we expect the effective mass of the excited quasiparticles will be smaller. Thus, we expect the aggregate effective mass to decrease as Q increases. Also, as the temperature is increased quasiparticles further from the Fermi surface can participate in $S(Q,\omega)$. At a given Q, there will be a temperature dependence[22] of $S(Q,\omega)$ arising from the enhancement of $m^*(\epsilon)$ at ϵ_F.

The paper is organized as follows. Section II introduces the enhanced mass model, where $m^*(k)$ peaks to $m^* = 2.8m_3$ at k_F. This peaking of m^* at k_F has not generally been included in models of $S(Q,\omega)$.[25] In a Brief Report[31] we found that this model described the Q dependence of the spin-dependent component $S_I(Q,\omega)$ and the density component $S_c(Q,\omega)$ of $S(Q,\omega)$ well at low temperature. In contrast, neither the ''Landau'' model,[32–34] with m^* fixed at $m^* = 2.8m_3$ for $Q \leqslant 1.6$ Å^{-1}, nor the paramagnon model,[35] with $m^* = m_3$, reproduces $S_I(Q,\omega)$ at all ω.[28] In addition, if $m^* = m_3$, there would be no zero-sound mode in $S_c(Q,\omega)$ at $Q \gtrsim 0.5$ Å^{-1} whereas a mode is observed up to $Q = 1.3$ Å^{-1}. In the present paper we explore how well the enhanced mass model can describe more precise data on the wave vector and temperature dependence of $S(Q,\omega)$ as well as the specific heat and the static susceptibility of liquid ^{3}He. Section III presents new neutron inelastic scattering measurements of $S(Q,\omega)$ in normal liquid ^{3}He at saturated vapor pressure for two temperatures, $T = 0.1$ K and $T = 1.4$ K, which is well below and close to the Fermi temperature T_F, respectively. Due to a new sample geometry, these measurements extend previous measurements to lower wave vectors and energies. In Sec. IV, we compare $S(Q,\omega)$ calculated from the enhanced mass model with the data at two different temperatures. Calculations of $C_V(T)$ and $\chi(T)$ are compared with the measured quantities in Sec. V. The meaning of the results is discussed in Sec. VI.

II. $S(Q,\omega)$ AND MODEL $m^*(k)$

A. Dynamic susceptibility

The inelastic neutron scattering cross-section for ^{3}He as a function of the momentum $\hbar Q$ and energy ω transferred to the liquid is proportional to the dynamic structure factor $S(\mathbf{Q},\omega)$,[25,36,37] which is a weighted sum of the density $S_c(\mathbf{Q},\omega)$ and spin-density $S_I(\mathbf{Q},\omega)$ correlations,

$$S(\mathbf{Q},\omega) = S_c(\mathbf{Q},\omega) + \frac{\sigma_i}{\sigma_c} S_I(\mathbf{Q},\omega), \tag{1}$$

where σ_c (σ_i) is the (in)coherent cross section. To evaluate $S_{c,I}(\mathbf{Q},\omega)$ it is convenient to introduce a corresponding dynamic susceptibility $\chi_{c,I}(\mathbf{Q},\omega)$. For example, at $T = 0$ K the spin dependent $\chi_I(\mathbf{Q},t)$ is

$$\chi_I(\mathbf{Q},t) = -\frac{1}{V}\langle T_t \rho_z(\mathbf{Q},t)\rho_z(\mathbf{Q},0)\rangle, \tag{2}$$

where T_t is a time ordering operator, V is the volume, and $\rho_z(\mathbf{Q},t) = \rho_\uparrow(\mathbf{Q},t) - \rho_\downarrow(\mathbf{Q},t)$ is the spin density. A similar expression is obtained for $\chi_c(\mathbf{Q},t)$ with $\rho_z(\mathbf{Q},t)$ replaced by the density $\rho(\mathbf{Q},t) = \rho_\uparrow(\mathbf{Q},t) + \rho_\downarrow(\mathbf{Q},t)$.

Writing $\rho_\uparrow(\mathbf{Q},t) = \Sigma_{\mathbf{k}} a^\dagger_{\mathbf{k}+\mathbf{Q}\uparrow}(t) a_{\mathbf{k}\uparrow}(t)$ as a sum of single-particle ($a^\dagger_{\mathbf{k}+\mathbf{Q}}$) and hole ($a_{\mathbf{k}}$) excitation states, $\chi_{c,I}(\mathbf{Q},\omega)$ can be expressed as[25]

$$\begin{aligned}\chi_{c,I}(\mathbf{Q},\omega) &= \int \frac{d^3k_1}{(2\pi)^3}\frac{d\omega_1}{2\pi} \\ &\quad \times \int \frac{d^3k_2}{(2\pi)^3}\frac{d\omega_2}{2\pi}\chi_{c,I}(\mathbf{k}_1\omega_1,\mathbf{k}_2\omega_2;\mathbf{Q}\omega) \\ &\equiv \int d\bar{1}d\bar{2}\chi_{c,I}(\bar{1}\bar{2},\mathcal{Q}),\end{aligned} \tag{3}$$

where $1 \equiv \mathbf{k}_1,\omega_1$ are the wave vector and energy of single-particle states involved, $\bar{1}$ means there is an integration over 1, and $\mathcal{Q} = \mathbf{Q},\omega$. An exact equation for $\chi(12,\mathcal{Q})$ can be readily derived in terms of free propagation of particle-hole pairs $\chi^0(1,\mathcal{Q})$ and the full interaction between pairs $I(12,\mathcal{Q})$,[25]

$$\chi_{c,I}(12,\mathcal{Q}) = \chi^0(1,\mathcal{Q})(2\pi)^4\delta(1-2) + \chi^0(1,\mathcal{Q})\int d\bar{3}I^{s,a}(1\bar{3},\mathcal{Q})\chi_{c,I}(\bar{3}2,\mathcal{Q}), \tag{4}$$

where I^s and I^a are the spin-symmetric and spin-antisymmetric interactions, respectively.

To evaluate $\chi_{c,I}(\mathbf{Q},\omega)$ we assume that $I(12,\mathcal{Q})$ is independent of the particle-hole indices 1 and 2, $I(12,\mathcal{Q}) \simeq I(\mathcal{Q}) = I(\mathbf{Q},\omega)$. The full equation, Eqs. (3) and (4), then reduces to the random-phase approximation (RPA)

$$\chi_{c,I}(\mathbf{Q},\omega) = \frac{\chi_0(\mathbf{Q},\omega)}{1 - I_{s,a}(\mathbf{Q},\omega)\chi_0(\mathbf{Q},\omega)}, \tag{5}$$

where $\chi_0(\mathbf{Q},\omega) = \int d\bar{1}\chi^0(\bar{1},\mathcal{Q})$ represents independent particle-hole propagation. We also assume that the single-particle energy $\epsilon(k,\omega)$ can be approximated by its on-shell energy $\epsilon(k,\omega) \simeq \epsilon(k,\epsilon_k) \equiv \epsilon_k$ so that $\chi_0(\mathbf{Q},\omega)$ reduces to the Lindhard function

$$\chi_0(\mathbf{Q},\omega) = \frac{2}{V}\sum_{\mathbf{k}} \frac{n_{\mathbf{k}} - n_{\mathbf{k+Q}}}{\omega + i\eta - (\epsilon_{\mathbf{k+Q}} - \epsilon_{\mathbf{k}})}, \tag{6}$$

where n_k is the Fermi function, $n(\epsilon_k)$. The $\chi_{c,I}(\mathbf{Q},\omega)$ are related to $S_{c,I}(\mathbf{Q},\omega)$ by

$$S_{c,I}(Q,\omega) = -\frac{1}{n\pi}[n_B(\omega)+1]\chi''_{c,I}(Q,\omega), \tag{7}$$

where we have replaced $\mathbf{Q}$ by Q since normal liquid ^{3}He is isotropic. In Eq. (7), $n = N/V$ is the number density and $n_B(\omega) = [\exp(\omega/k_BT)-1]^{-1}$ is the Bose function. Our model consists of a model for ϵ_k and $I_{s,a}(Q,\omega)$.

B. Model $m^*(k)$

We introduce a simple two-parameter model describing the peaking of the total effective mass $m^*(k)$ at the Fermi surface as calculated microscopically. The model $m^*(k)$ takes its maximum value $m^* = 2.8m_3$, the observed Landau effective mass, at $k = k_F$, and drops to a lower value m_0 (first parameter) away from k_F at a rate determined by f (second parameter). In units of the bare ^{3}He mass m_3, the model is

$$m^*(k) = m_0 + \frac{(m^* - m_0)}{2}\left[1 + \cos\left\{\frac{(k-k_F)\pi}{fk_F}\right\}\right] \tag{8}$$

for $(1-f)k_F < k < (1+f)k_F$ and $m^*(k) = m_0$ elsewhere. The model is displayed in Fig. 1. Essentially, $m^*(k)$ equals m_0 except for a small region $|k-k_F| < fk_F$ around k_F.

Given $m^*(k)$, the single-particle energy is defined as

$$\frac{d\epsilon_k}{dk} = \frac{\hbar}{m_3}\frac{k}{m^*(k)} \tag{9a}$$

or

$$\epsilon_k = \frac{\hbar}{m_3}\int_0^k dk' \frac{k'}{m^*(k')} + u_0. \tag{9b}$$

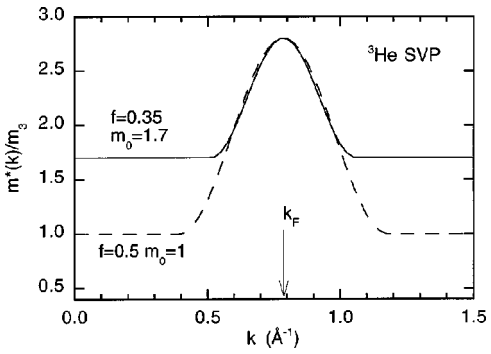

FIG. 1. The model effective mass $m^*(k)$ for parameters $f = 0.35$ and $m_0 = 1.7$ (solid line) and $f = 0.5$ and $m_0 = 1$ (dashed line). The Fermi wave vector k_F is shown by the arrow.

With definition (9), $m^*(k)$ is the total effective mass, i.e., the product of the ω mass and the k mass,[2,38]

$$m^*(k) = m^*_\omega m^*_k. \tag{10}$$

Generally, calculations find that m^*_k is largely independent of k.[2,12,13,24] The change in m^* as we move off the Fermi surface arises from the energy dependence of m^*_ω.[2,12,13] The separation is not important here because we use on-shell energies only, $\epsilon(k,\omega) = \epsilon(k,\epsilon_k)$. Also, since energy differences only enter $\chi_0(Q,\omega)$, the value of u_0 is unimportant.

The values of the parameters for $m^*(k)$ were determined from earlier neutron-scattering measurements by Fåk and Glyde[31] as $f = 0.35$ and $m_0 = 1.7$. Examples of $\epsilon(k)$ calculated from Eq. (9b) and of the noninteracting dynamic susceptibility $\chi_0(Q,\omega)$ calculated from Eq. (6) using the model $m^*(k)$ are given in Ref. 31.

C. Interaction

In the limit $Q \to 0$ and $T \to 0$ particle-hole excitations immediately at the Fermi surface only are excited, as in thermodynamic properties at $T \to 0$. In this case both $\mathbf{k}_1, \omega_1$ and $\mathbf{k}_2, \omega_2$ are at k_F, ϵ_F, the approximation $I(12,\mathcal{Q}) = I(\mathcal{Q})$ is exact, and $I(\mathcal{Q})$ reduces to the Landau theory interaction[25,39]

$$\left(\frac{dn}{d\epsilon}\right)I_{s,a}(\mathbf{Q},\omega) = F_0^{s,a}(Q) + \frac{F_1^{s,a}(Q)}{1 + F_1^{s,a}(Q)/3}\left(\frac{\omega}{v_F Q}\right)^2, \tag{11}$$

where $(dn/d\epsilon) = m^*k_F/\pi^2\hbar$ is the density of states per unit volume for both spins at the Fermi surface. This interaction is exact only at $T \to 0$ and $Q \to 0$ and low ω. In this limit $F^{s,a}_{0,1}(Q)$ reduce to the Landau parameters $F^{s,a}_{0,1}$. $F^{s,a}_{0,1}$ are obtained empirically from observed thermodynamic properties at $T \to 0$ K.[6]

There are several first-principles calculations of the particle-hole interaction $I(\mathcal{Q})$ at finite Q and ω.[12,40,41] In general, I is very complicated because it depends on $\mathbf{k}_1\omega_1$, $\mathbf{k}_2\omega_2$ as well as Q and ω. However, the Q dependence of the Landau parameters can be evaluated. Essentially, $F^s_0(Q)$ is found to be independent of Q up to $Q \simeq 0.5$ Å^{-1}, to increase somewhat with Q up to $Q \simeq 1$ Å^{-1}, and then drop rapidly to zero at $Q \sim 1.7$ Å^{-1} and oscillate at high Q. This Q dependence results from the interaction via the hard core whereas the large positive value of

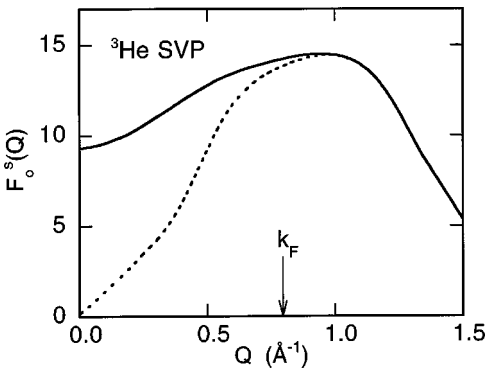

FIG. 2. The Q dependence of $F_0^s(Q)$ used in the model (solid line) is based on the microscopic calculations in Ref. 11 (dotted line), constrained to reproduce the Landau parameter $F_0^s=9.3$ in the limit $Q\rightarrow 0$.

$F_0^s=9.3$ at $Q\rightarrow 0$ arises from interactions via the collective excitations. $F_0^s(Q)$ has also been determined empirically[32] by fitting to the observed zero-sound mode, providing a good test for microscopic calculations. F_0^a is found to change little with Q.[12] Little is known microscopically about the Q dependence of $F_1^{s,a}(Q)$.

We choose $F_{0,1}^{s,a}(Q=0)=F_{0,1}^{s,a}$, the Landau parameters,[20] so that $I_{s,a}(Q,\omega)$ reduces to the Landau interaction at $Q\rightarrow 0$. In this way with $m^*(k_F)=m^*=2.8m_3=(1+F_1^s/3)$, the model reduces exactly to Landau theory at $Q\rightarrow 0$ and will therefore reproduce low-temperature thermodynamic properties. For the Q dependence of $F_0^s(Q)$ we use the solid line shown in Fig. 2, as calculated by Clements *et al.*[12] with $F_0^s(Q=0)$ constrained to $F_0^s=9.3$. $F_1^s(Q)$ is chosen so that the f-sum rule is fulfilled using $m^*(k)$ in Eq. (8). Following microscopic calculations,[12] $F_0^a(Q)$ is taken independent of Q. $F_1^a(Q)$ is also taken independent of Q and we use $F_0^a=-0.695$ and $F_1^a=-0.55$ at saturated vapor pressure.[20]

III. MEASUREMENTS OF $S(Q,\omega)$

A. Experimental procedure

Neutron inelastic scattering measurements were performed on the IN6 time-of-flight spectrometer installed on a cold neutron guide at the high-flux reactor of the Institut Laue-Langevin. The main advantages with this spectrometer is the high neutron flux, the good energy resolution, the large solid angle, and the low background. An incident energy of 3.1 meV was chosen as a compromise between energy resolution, flux, and kinematical range. It also offers the advantage that Bragg scattering from aluminum is impossible, thus reducing the background. The energy resolution for elastic incoherent scattering was 77 μeV and energy transfers between -1 and 2.5 meV were recorded.

All previous cold neutron-scattering measurements on liquid ^{3}He have been performed in reflection geometry, due to the enormous absorption cross section of the ^{3}He nucleus. However, this geometry is not suitable for small scattering angles (small wave-vector transfers), and we have therefore chosen to work in transmission geometry. This has the additional advantage that a smaller cell with a smaller amount of liquid ^{3}He can be used, and the disadvantages of a lower

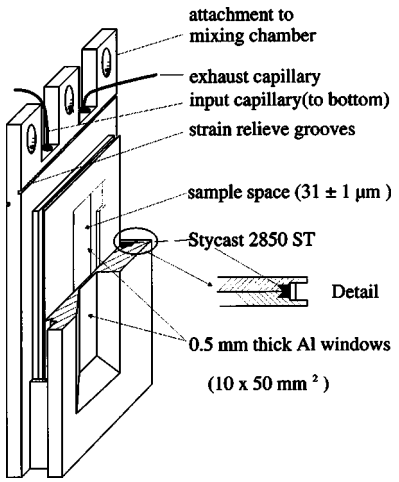

FIG. 3. Sample cell for transmission measurements. The beam comes in from the rear and scatters out towards the reader.

scattering probability, a restricted angular range (in the present case where the cell window was oriented perpendicular to the neutron beam, the scattering angle was in the range $15<\phi<60°$), and difficulties in making such a sample cell. For the incident energy chosen, the optimal cell thickness is only 31 μm with a tolerance and flatness better than 2 μm. The windows of the cell should be as thin as possible to decrease the amount of incoherent elastic scattering, and at the same time thick enough that the elastic deformation of the cell does not exceed 2 μm. Different materials were tested, and the final choice, a relatively pure cold-worked aluminum alloy ($\sim$0.6% Mg and $\sim$0.5% Si), was chosen as a compromise between purity (small incoherent scattering), mechanical stiffness, and ease of machining. The cell (see Fig. 3) was made from two pieces, which were pressed together and glued with Stycast 2850 FT from the outside, to ensure the right thickness of the sample space. Before gluing, the sample cavity and the 0.5-mm-thick windows were machined by electroerosion. The effective sample area was 5 cm^2. The thickness (30.6 ± 1.0 μm) and homogeneity were measured by neutron transmission, with the cell filled with liquid ^{3}He at low temperatures. The cell was scanned through a 2-mm-diam beam with steps of 1 mm in the two directions, using 4 Å neutrons at the Braunschweig reactor. We also examined the elastic ($\sim$7 μm/bar) and plastic (none) deformation of the cell windows as a function of filling pressure, since the elastic constants of aluminum are not well known at low temperatures.

Two filling capillaries were connected to the cell, as well as a calibrated carbon thermometer. An elaborate system of cadmium shields including a beam dump was attached to the cell in order to reduce the background. The cell was mounted in a dilution refrigerator with a base temperature of 5 mK. A small magnetic field of at least 80 mT from Co-Sm permanent magnets attached to the cell quenched the aluminum to the nonsuperconducting state, thereby improving the thermal conductivity. The temperature of the sample cell and the mixing chamber of the dilution refrigerator was lower than 18 mK with the neutron beam closed. With the beam open, the temperature of the sample cell raised to 30 mK and the mixing chamber to 25 mK. The beam heating is dominated by γ radiation, which is of the order of 8 μW. Less than 1%

of this heat reaches the sample; the rest is effectively evacuated by the cell to the mixing chamber. Neutron absorption by the ^{3}He nuclei produces 30 nW of heat. While the temperature gradient within the ^{3}He sample is negligible, the Kapitza resistance between the liquid ^{3}He and the normal-state aluminum is such that the temperature of the ^{3}He sample raised to a temperature of about 100 mK. This is similar to the temperature measured in our previous experiment.[27,28] While we can only make an estimate of the lowest temperature in the present experiment, it is clear from the detailed-balance condition of the neutron scattering cross section that the temperature cannot be higher than 0.3 K.

Measurements were performed at saturated vapor pressure (SVP) at two temperatures 0.1 and 1.4 K, the latter being close to the Fermi temperature of $T_F \approx 1.77$ K. The scattering from the empty can at low temperatures was measured before and after the helium measurements. In order to have sufficiently good statistics for a line-shape analysis, the duration of each of these measurements was of the order of 3.5 days. The scattering from a vanadium sample, in a geometry identical to that of the ^{3}He sample and mounted below the ^{3}He sample cell, was measured on a regular basis by raising the cryostat in the beam, in order to detect any changes of the detector efficiencies as a function of time.

A consistency check was made on all data collected, following the lines of Ref. 42, and discussed in the Appendix. This allows to identify detectors that are *inconsistently* noisy, and runs that have particular problems. Data were then added into 45 angular detector groups and normalized to the monitor count rate and the incoherent scattering from vanadium. The scattering from the empty cell outside the elastic peak was smoothed by a running average and subtracted from the sample runs. The treatment of the elastic peak was somewhat more complicated, since the peak is weaker in the full can due to absorption by the ^{3}He nuclei. We used the following procedure: The elastic peak in the sample runs was fitted by a Gaussian, with only the height as a free parameter. The peak position and the peak width were obtained from similar fits to the empty can. Although there is no strictly elastic scattering from liquid ^{3}He at low temperatures, spin fluctuations contribute at small energies, and the fit was therefore performed only on the left-hand side of the peak (including the first point on the right-hand side). This Gaussian was then subtracted from the data. Conversion from time of flight to energy transfer and absorption corrections were made following standard procedures. We note in passing that transmission geometry has an advantage compared with reflection geometry in that the absorption correction is not extremely sensitive to the exact orientation of the cell with respect to the beam direction. The data at constant scattering angle were rebinned to constant Q,[43] using $\Delta Q = 0.1$ Å^{-1} and $\Delta\omega \geqslant 0.02$ meV. A coherent scattering cross section of $\sigma_c = 4.42$ b was used to obtain the dynamical structure factor $S(Q,\omega)$ in absolute units [cf. Eq. (1)].

B. Experimental results

Figure 4 shows the present data at $Q = 0.5$ Å^{-1} (upper frame) compared with previous data (lower frame). The present data are in excellent agreement with previous results,[28] and give considerably more information on the line

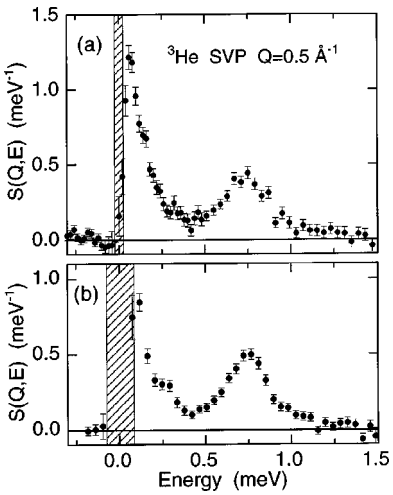

FIG. 4. Comparison of $S(Q,\omega)$ for (a) the present experiment using a transmission cell with thin windows and (b) an earlier experiment (Refs. 27 and 28) where a high-pressure cell in reflection geometry with thick windows was used. The hatched area corresponds to the ''blind'' region around the elastic peak. The reduction of the elastic scattering allows a better determination of the low-energy spin-fluctuation scattering in case (a).

shape of the low-energy spin-fluctuation peak. This is because the elastic scattering from the present sample cell is a factor of 20 less than that from previous cells due to the thin windows. Lower Q values can also be observed using a transmission cell.

Figure 5 shows the dynamic structure factor $S(Q,\omega)$ as a function of energy ω for Q values $0.3 \leqslant Q \leqslant 0.8$ Å^{-1} at $T = 0.1$ and 1.4 K. The peak at high energies is the zero-sound mode, which depends only weakly on temperature, even up to temperatures close to the Fermi temperature. The peak at low energies is the spin-fluctuation scattering, which in contrast broadens substantially with increasing temperature.

In order to analyze the data and extract observed values of the zero-sound-mode energy ω_Q, width Γ_Q, and weight Z_Q, a model for the total $S(Q,\omega)$ was convoluted with the instrumental resolution function and fitted to the data. This model consists of two contributions [cf. Eq. (1)]: spin fluctuations in $S_I(Q,\omega)$, whose line shape is calculated using the enhanced mass model (see Sec. II), and zero sound in $S_c(Q,\omega)$, described by a damped harmonic oscillator (DHO) function

$$S_c(Q,\omega) = \frac{1}{\pi}[n_B(\omega)+1]\frac{4\omega\omega_Q Z_Q \Gamma_Q}{(\omega^2-\Omega_Q^2)^2+4\omega^2\Gamma_Q^2}. \quad (12)$$

Here $\Omega_Q = (\omega_Q^2+\Gamma_Q^2)^{1/2}$ is interpreted as the energy of the zero-sound mode, $2\Gamma_Q$ is the width [full width at half maximum (FWHM)], and Z_Q is the weight. The solid lines in Fig. 5 show the fits of the enhanced mass model for $S_I(Q,\omega)$ and of the DHO function for $S_c(Q,\omega)$ which contains only four parameters that are fitted to the data: three for the zero-sound mode, Ω_Q, Γ_Q, and Z_Q, for which observed values are sought, and one for the spin fluctuations, the overall scale factor σ_i/σ_c in Eq. (1). The latter quantity is not precisely known, but the values obtained from the fits are within the values quoted in the literature, i.e., between 0.25 and 0.36.

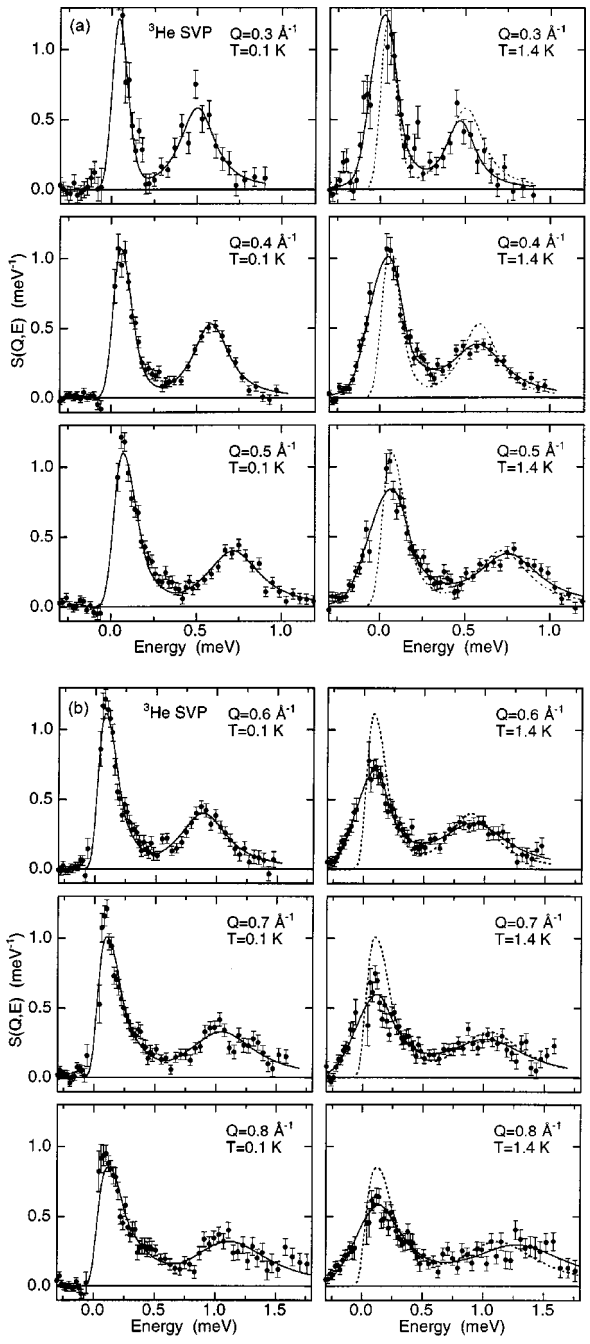

FIG. 5. Total dynamic structure factor $S(Q,\omega)$ of liquid ^{3}He at SVP for different wave vectors at two temperatures. Dots with error bars are experimental data from this work. The solid line is a fit to the sum of the spin-fluctuation scattering (low-energy peak), modeled by an effective mass $m^*(k)$ that is peaked at k_F, and a damped harmonic oscillator at higher energies describing the zero-sound mode. The dotted line on the right-hand (high-temperature) side shows the low-temperature fit.

The experimental results for the zero-sound mode energy, width, and weight in $S(Q,\omega)$ obtained from these fits, given in Table I, are in excellent agreement with earlier experimental results at low temperatures.[28] The integrated intensity of the zero-sound mode is nearly equal to the static structure factor $S_c(Q)$, which confirms earlier observations that multiparticle excitations in the coherent scattering cross section are negligible for $Q<0.8$ Å^{-1}. In the temperature range $0.1\leqslant T\leqslant 1.4$ K, the energy Ω_Q and weight Z_Q of the mode are essentially independent of temperature. The width Γ_Q, which is approximately proportional to Q^2 at both low and high temperatures, increases significantly with temperature, as shown in Fig. 6.

IV. ENHANCED MASS MODEL OF $S(Q,\omega)$

The goal of this section is to test how well the enhanced mass model of $S(Q,\omega)$ presented in Sec. II agrees with experiment.

A. Low temperatures

To evaluate the coherent $S_c(Q,\omega)$ and zero-sound properties at low temperatures, we note that the zero-sound mode occurs at the energy ω at which the denominator of $\chi_c(Q,\omega)$ in Eq. (5) vanishes, i.e., at $I_s(Q,\omega)\mathrm{Re}\,\chi_0(Q,\omega)=1$. The input in the calculation is the Landau interaction (11) and $\chi_0(Q,\omega)$ in Eq. (6), obtained using quasiparticle energies ϵ_k, Eq. (9), and from the enhanced mass model $m^*(k)$, Eq. (8), using $f=0.35$ and $m_0=1.7$ as in Ref. 31. The resulting zero-sound mode energy $\omega=\Omega_Q$ is shown in Fig. 7. The agreement with experiment at $T=0.1$ K up to $Q=0.8$ Å^{-1} is excellent. Good agreement at higher Q values is not expected because multipair contributions, which are not included in the present model, become important for $Q>0.8$ Å^{-1}. The weight Z_Q of the zero-sound mode in $S_c(Q,\omega)$ is given from Eq. (5) by

$$Z_Q=-\frac{1}{n}\frac{\mathrm{Re}\,\chi_0(Q,\Omega_Q)}{\dfrac{\partial}{\partial\omega}[I_s(Q,\omega)\mathrm{Re}\,\chi_0(Q,\omega)]_{\omega=\Omega_Q}}. \qquad (13)$$

This expression has been evaluated numerically and the resulting Z_Q is also in good agreement with the observed Z_Q, as shown in Fig. 7.

Since the spin-symmetric interaction $I_s(Q,\omega)$ is positive and large, the zero-sound mode lies at high energies, above the single particle-hole band. Thus, in the present model, the zero-sound mode cannot decay to single particle-hole pairs, and the calculated width Γ_Q is negligible. To evaluate $S_c(Q,\omega)$ we have used the calculated Ω_Q and Z_Q in a DHO function and taken Γ_Q from experiment. The resulting

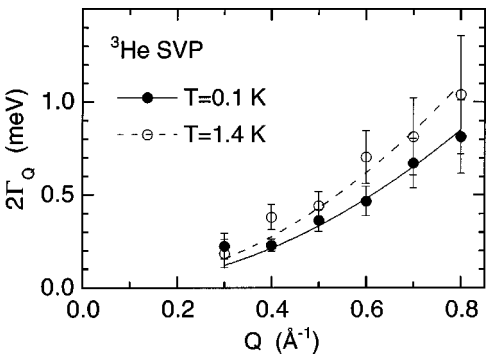

FIG. 6. Measured width $2\Gamma_Q$ (FWHM) of the zero-sound mode as a function of wave vector Q at temperatures of $T=0.1$ K (solid symbols) and $T=1.4$ K (open symbols). The lines are fits to $\Gamma_Q=CQ^2$.

TABLE I. Experimental results for the energy Ω_Q, width (FWHM) $2\Gamma_Q$, and weight Z_Q of the zero-sound mode. Values in parentheses are statistical errors (one standard deviation).

	Ω_Q(meV)		$2\Gamma_Q$(meV)		Z_Q	
Q(Å^{-1})	$T=0.1$ K	$T=1.4$ K	$T=0.1$ K	$T=1.4$ K	$T=0.1$ K	$T=1.4$ K
0.3	0.52 (2)	0.48 (3)	0.22 (7)	0.18 (8)	0.22 (5)	0.15 (5)
0.4	0.60 (1)	0.60 (2)	0.23 (3)	0.38 (7)	0.20 (2)	0.24 (3)
0.5	0.74 (2)	0.78 (3)	0.36 (6)	0.44 (8)	0.24 (3)	0.27 (3)
0.6	0.92 (3)	0.97 (5)	0.47 (8)	0.70 (14)	0.30 (4)	0.38 (5)
0.7	1.10 (5)	1.09 (7)	0.67 (13)	0.81 (21)	0.36 (5)	0.37 (6)
0.8	1.18 (7)	1.37 (11)	0.81 (20)	1.04 (32)	0.43 (6)	0.51 (9)

$S_c(Q,\omega)$ makes up the high-energy (zero-sound) part of the total $S(Q,\omega)=S_c(Q,\omega)+(\sigma_i/\sigma_c)S_I(Q,\omega)$ [cf. Eq. (1)] which is shown for $T=0.1$ K by the solid line on the left-hand side of Fig. 8. The energy range and weight of $S_c(Q,\omega)$ agree well with experiment for all wave vectors $0.3\leqslant Q\leqslant 0.8$ Å^{-1}.

The spin-dependent dynamic structure factor $S_I(Q,\omega)$ is evaluated using Eqs. (5)–(7) and (11) with the enhanced effective mass $m^*(k)$ from Eq. (8), using the same parametrization as for the zero-sound mode above. $S_I(Q,\omega)$ makes up the low energy (spin-fluctuation) part of $S(Q,\omega)$, where we have used $\sigma_i/\sigma_c=0.33$. The total $S(Q,\omega)$ at $T=0.1$ K (solid line on the left-hand side of Fig. 8) is in excellent agreement with the present experimental data.

B. High temperatures

We have evaluated the temperature dependence of both the density and spin-density response within the mass-enhanced model. In the calculation, the temperature enters only through the Fermi distribution function $n_{\mathbf{k}}$ in Eq. (6) and the Bose factor in Eq. (7). There are no adjustable parameters at high temperatures. It is worth mentioning that the calculations of the high-temperature behavior were actually carried out before the present experiment. The calculated $S_I(Q,\omega)$ is in excellent agreement with measurements at $T=1.4$ K, as shown on the right-hand side of Fig. 8. Both the ω dependence and the overall intensity of $S_I(Q,\omega)$ come out well in the calculation. This is a quite remarkable result, since the temperature dependence of $S_I(Q,\omega)$ is caused by a nontrivial interplay between the population (Bose) factor and the T dependence of the noninteracting susceptibility, $\chi_0(Q,\omega)$.[30]

The good agreement of the $m^*(k)$ model with the temperature dependence of $S_I(Q,\omega)$ is in stark contrast to models using a constant effective mass, such as the paramagnon model ($m^*=1$) or the Landau model ($m^*=2.8$). These latter models, which both fail to describe the ω dependence of the observed $S_I(Q,\omega)$ at low temperatures,[28] are in serious disagreement with the data at high temperatures. This is illustrated in Fig. 9, where $S_I(Q,\omega)$ calculated using the three models in which all model parameters are held the same at low and high temperatures are compared with experiment. The paramagnon and Landau models completely overestimate the intensity of $S_I(Q,\omega)$ at high temperatures, and the overall shape is not well described. A slight overestimate of the intensity at high temperatures in the $m^*(k)$ model can be seen.

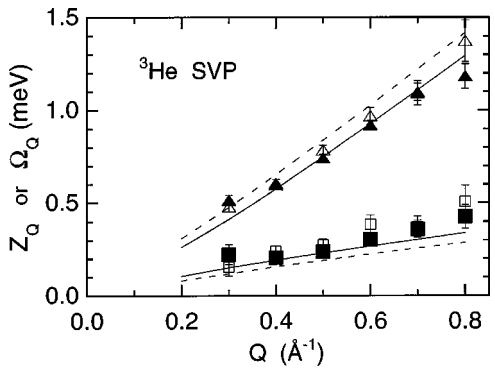

FIG. 7. Measured energy Ω_Q (triangles) and weight Z_Q (squares) of the zero-sound mode as a function of wave vector Q at temperatures of $T=0.1$ K (solid symbols) and $T=1.4$ K (open symbols). Calculated quantities using the enhanced mass model $m^*(k)$ described in the text are given by solid lines at $T=0.1$ K and dashed lines at $T=1.4$ K.

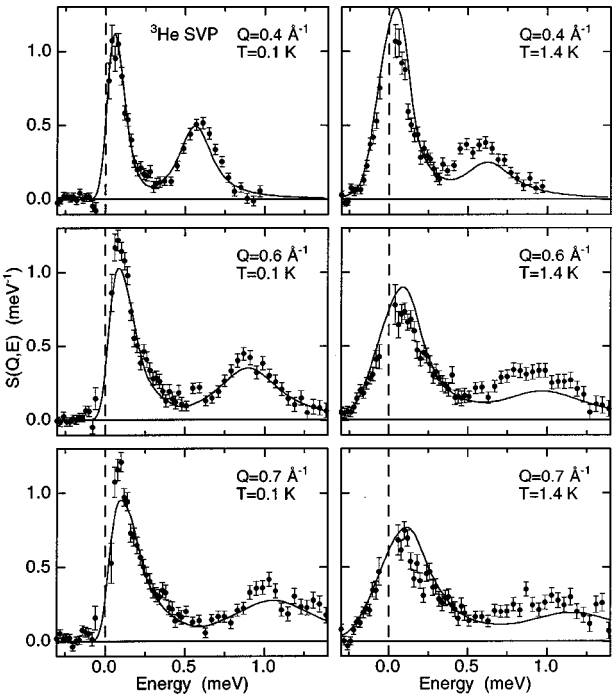

FIG. 8. Comparison of the calculated total dynamic structure factor $S(Q,\omega)$ (lines) using the enhanced mass model with experimental data (dots) of liquid ^{3}He at SVP for different wave vectors at two temperatures. The model contains no adjustable parameters.

The predicted temperature dependence of the energy and weight of the zero-sound mode is in good overall agreement with experiment (Fig. 7). However, the model predicts an increase in the energy of the zero-sound mode between $T=0.1$ and 1.4 K, which is not observed. This discrepancy may be related to the lack of damping in the enhanced mass model. Increased damping is observed at $T=1.4$ K and interactions leading to damping also tend to decrease the mode energy. As expected, the amount of Landau damping (decay of the zero-sound mode into particle-hole excitations) in the model cannot describe the observed broadening of the zero-sound mode even at low temperatures. The contribution of multiparticle excitations to the damping[34,44,45] is believed to be of great importance, as suggested by the pressure dependence of Γ_Q.[28] Also, we expect the Landau parameters to ''soften'' somewhat with increasing temperature as the zero-sound mode and paramagnon resonances broaden. This effect is not included here. The softening of the interaction will reduce the zero-sound-mode energy.

V. SPECIFIC HEAT AND MAGNETIC SUSCEPTIBILITY

A. Specific heat

In this section we test how well our model of $m^*(k)$ can reproduce the observed temperature dependence of the specific heat, $C_V(T)$. As noted, the temperature dependence of C_V is very complicated containing many competing contributions. The contribution to C_V arising from the peaking of $m^*(k)$ has been considered previously by Brown *et al.*[16] and Fantoni *et al.*[24] using a model of $m^*(k)$ proposed for nuclei by Brown and Rho.[46]

At very low temperatures, the excitations of a Fermi liquid are well described as excitations of independent quasiparticles. As shown initially by Landau, C_V is given by the simple Fermi gas result with the bare mass replaced by the effective mass m^* of quasiparticles on the Fermi surface,[5,6]

$$C_V=\frac{\pi^2}{3}\left(\frac{dn}{d\epsilon}\right)k_B^2T=\frac{m^*k_F}{3\hbar}k_B^2T=\frac{\pi^2}{2}Nk_B\frac{T}{T_F^*}. \qquad (14)$$

In liquid ^{3}He, deviations from Eq. (14) are evident at $T\simeq 10$ mK. These deviations are well described by contributions to C_V proportional to $T^3\ln T$ and which have been investigated in depth.[14,16–18,21–23] Contributions to $C_V(T)$ arising from cooperative excitations have this T dependence, e.g., the C_V of electrons in metals arising from coupling of electrons to phonons, the C_V of electrons in weakly ferromagnetic materials arising from spin fluctuations, and the C_V of liquid ^{3}He arising from spin fluctuations and possibly phonons. The $T^3\ln T$ temperature dependence holds in ^{3}He up to $T\simeq 50$–100 mK. At higher temperatures $C_V(T)$ is more complicated.

In our case, a second complication arises. The single-particle energies used in $S(Q,\omega)$ are ''dynamical'' quasiparticle energies, since in $S(Q,\omega)$ they are the real part of poles of the single-particle propagators. The energies appearing in C_V are ''statistical'' quasiparticle energies, defined as derivatives of the free energy. The two energies are not the same.[2,21–23] Since we have initiated our model ϵ_k to describe $S(Q,\omega)$, this ''defines'' our model ϵ_k as ''dynamical'' quasiparticle energies. Carneiro and Pethick[22] have evaluated the difference between the two ϵ_k exactly but their results hold up to approximately 100 mK only. We wish to go up to $T\simeq 1.5$ K. In our calculations we have simply ignored this difference.

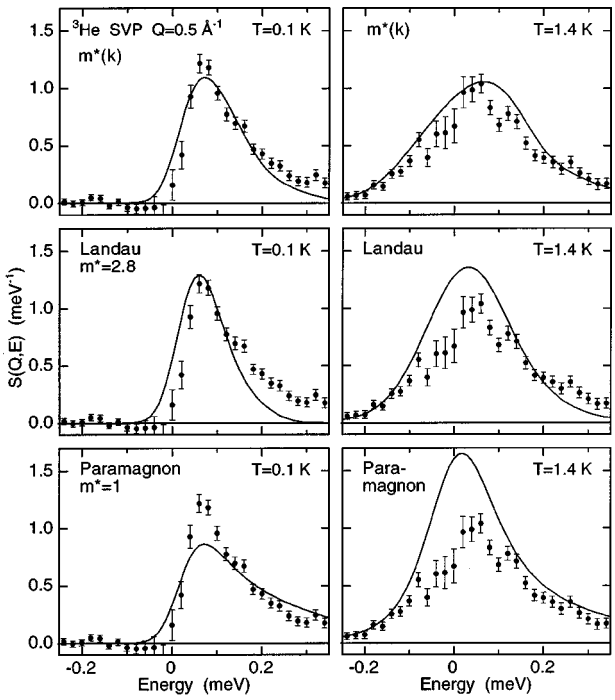

FIG. 9. $S_I(Q,\omega)$ in liquid ^{3}He at $Q=0.5$ Å^{-1} calculated for different models at $T=0.1$ K (left-hand side) and $T=1.4$ K (right-hand side). The mass-enhanced model (top) uses a k-dependent effective mass $m^*(k)$ with $f=0.35$ and $m_0=1.7$, the Landau model (middle) a constant effeective mass $m^*=2.8$, and the paramagnon model (bottom) uses $m^*=1$.

Third, the enhancement of m^* at k_F itself almost certainly decreases with increasing T. The enhancement of m^* arises in part from the existence of a well-defined or sharp spin-fluctuation resonance. At $T=1.4$ K, this resonance, as observed in $S_I(Q,\omega)$, is significantly broadened from its low T shape (see Fig. 5). Thus the enhancement of m^* at $T=1.4$ K is expected to be significantly reduced below its $T=0$ K value. This expected reduction of m^* with T is also not included here, as is apparently the case with all previous calculations.

Essentially, we evaluate the entropy for independent quasiparticles from

$$S=-\frac{k_B}{V}\sum_k\left[n_k\ln n_k+(1-n_k)\ln(1-n_k)\right], \qquad (15)$$

where

$$n_k=\left[e^{(\epsilon_k-\mu)/k_BT}+1\right]^{-1} \qquad (16)$$

is the Fermi function and ϵ_k is our model single-quasiparticle energy (8) and (9). The chemical potential $\mu(T)$ at each T was determined so that $N=\Sigma_k n_k$ remains constant. The $C_V(T)$ was obtained from $S(T)$ by numerical differentiation,

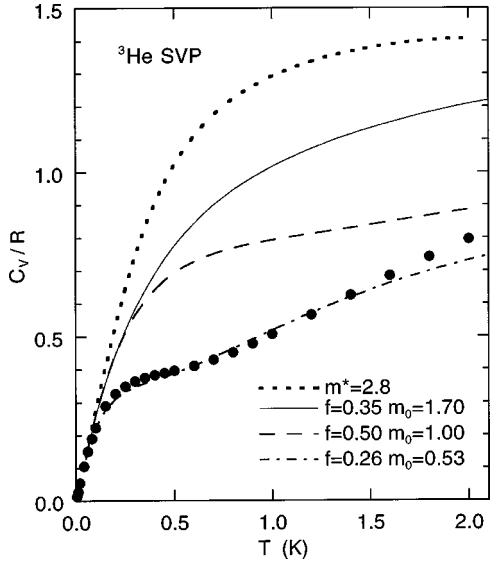

FIG. 10. Measured specific heat $C_V(T)$ (Ref. 19) (dots) as a function of temperature compared with $C_V(T)$ calculated using a free Fermi gas model $m^*=2.8$ (dotted line) and with the mass-enhanced model $m^*(k)$, Eq. (8), with $f=0.35$ and $m_0=1.7$ (solid line), with $f=0.5$ and $m_0=1$ (dashed line), and with best-fit values $f=0.26$ and $m_0=0.53$ (dash-dotted line).

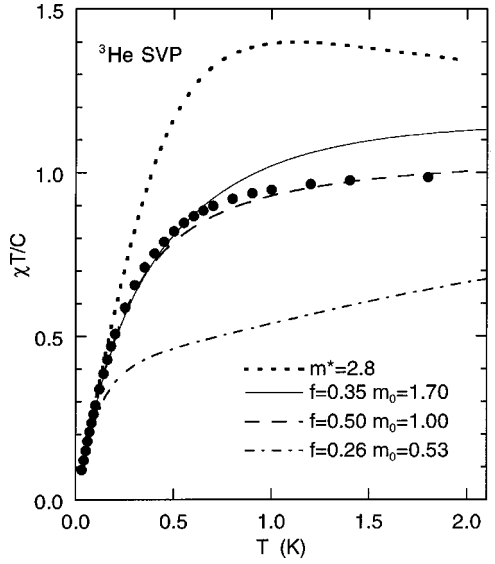

FIG. 11. Measured static magnetic susceptibility $\chi(T)$ (Ref. 47) (dots) multiplied by the temperature compared with $\chi(T)T$ calculated using a free Fermi gas model $m^*=2.8$ (dotted line) and with the mass-enhanced model $m^*(k)$, Eq. (8), with $f=0.35$ and $m_0=1.7$ (solid line), with $f=0.5$ and $m_0=1$ (dashed line), and with $f=0.26$ and $m_0=0.53$ (dash-dotted line), the values that give a good description of the specific heat.

$$C_V(T)=T\left(\frac{dS(T)}{dT}\right)_V. \tag{17}$$

Fantoni *et al.*[12] made exactly this calculation using the Brown-Rho model[46] of $m^*(k)$.

Figure 10 compares the observed[19] $C_V(T)$ with that calculated from Eqs. (15)–(17) using different quasiparticle dispersions ϵ_k. The observed $C_V(T)$ shows a marked ''bendover'' at $T\approx 0.2$ K that is not reproduced at all using the free Fermi gas energy $\epsilon_k=\hbar k^2/2m^*$ with $m^*=2.8$. As noted, $m^*=2.8$ is obtained by fitting Eq. (14) to the observed C_V at $T\to 0$ (Landau theory).[5,6,20] Calculations using the enhanced-mass model are shown for the following parameter values: $f=0.35$ and $m_0=1.7$, the values which reproduce $S(Q,\omega)$ well; $f=0.5$ and $m_0=1$, which give a marginally better description of $\chi(T)$ (see below); and $f=0.26$ and $m_0=0.53$, which give the best fit to the observed $C_V(T)$. All the calculated $C_V(T)$ agree with the observed data at $T\to 0$, since the model reduces to Landau theory at $T\to 0$. The pronounced ''bendover'' in the data at $T\simeq 0.2$ K can be reproduced by the model. However, the values of f and m_0, especially m_0, are quite different from those needed to reproduce $S(Q,\omega)$. The ''bendover'' in $C_V(T)$ is in fact produced by a small value of m_0. This means a large drop in $m^*(k)$ and a large increase in the excitation energy is needed in this model as we move a relatively small distance away from ϵ_F. For example, quasiparticles having an energy $\epsilon\gtrsim(\hbar/2m_3)(k_F/3)^2\sim 0.5$ K away from ϵ_F will have a mass $m^*=m_0$. Thus at $T\sim 0.5$ K the effective mass of quasiparticles excited is $m_0\simeq 0.5$, down rapidly from $m^*=2.8$ at $T\to 0$. This agrees with the findings of Fantoni *et al.*, who, using m_0 of 0.76 in the $m^*(k)$ of Brown and Rho, found a $C_V(T)$ that agreed well but lay somewhat above the observed $C_V(T)$ for $T\gtrsim 0.25$ K. Other factors not included here,[14,16,21] especially the drop in m^* itself with increasing T, could contribute significantly to the observed change in slope of C_V with increasing T. Such a low value of m_0 would then not be needed.

B. Magnetic susceptibility

The static magnetic susceptibility of a Fermi liquid at low temperatures is independent of temperature and given by Landau theory as[5,6]

$$\chi=\left(\frac{dn}{d\epsilon}\right)\frac{\beta^2}{1+F_0^a}=\frac{m^*k_F}{\pi^2\hbar}\,\frac{\beta^2}{1+F_0^a}, \tag{18}$$

where β is the magnetic moment of the ^{3}He nucleus. Compared to a Fermi gas, the susceptibility is enhanced by the factor $(m^*/m_3)/(1+F_0^a)$. In liquid ^{3}He at low temperatures and SVP, this enhancement factor is 9.18. At high temperatures, $\chi(T)$ is inversely proportional to the temperature, and it is therefore useful to plot the quantity χT vs temperature rather than $\chi(T)$ itself. The observed[47] $\chi T/C$ (C is the Curie constant) shown in Fig. 11 has the expected behavior: it is linear in T at low temperatures and constant at high T. The region $0.2\lesssim T\lesssim 1.5$ K is characterized by a crossover behavior.

In the standard Landau Fermi-liquid picture of ^{3}He, the effective mass $m^*=2.8$ is determined from the enhancement of the linear term in the specific heat and the Landau parameter F_0^a is obtained subsequently from the enhancement of the static susceptibility, using $m^*=2.8$. In the paramagnon model, m^* is set to 1, and F_0^a determined from the enhancement of the static susceptibility thus acquires a value closer to -1; i.e., the system is closer to a ferromagnetic instability. At finite temperatures, the principal correction term to the constant χ is a $-T^2$ term, which in the paramagnon

model is reinforced by low-energy spin fluctuations (paramagnons).[48] For temperatures above 0.2 K, even stronger deviations are observed.

The static susceptibility can be calculated from the dynamical susceptibility $\chi''(Q,\omega)$ as

$$-\chi(T)=\lim_{Q\to 0}\chi'(Q,\omega=0,T)=\lim_{Q\to 0}\frac{2}{\pi}\int_0^\infty d\omega\frac{\chi''(Q,\omega)}{\omega}, \tag{19}$$

where the prime ($'$), which denotes the real part, will be dropped in what follows, since $\chi''(Q,\omega)\to 0$ as $\omega\to 0$. Taking the static limit ($\omega\to 0$) of the RPA expression (5) and inserting into Eq. (19), we find for $Q\to 0$

$$-\chi^{-1}(T)=\chi_0^{-1}(0,0)-I_a(0,0)=\chi_0^{-1}(0,0)-F_0^a\left(\frac{dn}{d\epsilon}\right)^{-1}. \tag{20}$$

In the limit $Q\to 0$, only quasiparticles close to the Fermi surface will be involved, and we can expand n_k close to k_F so that

$$\chi_0(0,0)=\frac{2}{V}\sum_k\frac{dn}{d\epsilon}=\frac{1}{\pi^2}\int dk\,k^2\left(\frac{dn_k}{d\epsilon_k}\right)_k. \tag{21}$$

We have calculated the static susceptibility by numerically integrating this equation for all temperatures, using n_k from Eq. (16), with ϵ_k from Eqs. (8) and (9).

Figure 11 compares the observed[47] χT with that calculated from Eqs. (19)–(21), using different quasiparticle energies. The χ calculated using the free Fermi gas $\epsilon_k=\hbar k^2/2m^*$ with $m^*=2.8$ clearly overestimates the observed χ. Calculations using the enhanced-mass model with the parameters values $f=0.35$ and $m_0=1.7$, the values which reproduce $S(Q,\omega)$ well, are in excellent agreement with the temperature dependence of χT up to temperatures of the order of 0.6 K. Better agreement can be obtained by slightly different parameters $f=0.5$ and $m_0=1$. This parameter set gives also a good description of $S_I(Q,\omega)$, but $S_c(Q,\omega)$ comes out less well.[31] A nearly perfect fit can be obtained by using slightly different parameter values. It is remarkable that the simple concept of an effective mass $m^*(k)$ that is peaked at k_F can give such a good agreement with the observed $\chi(T)$ over a large temperature interval. However, the parameter values $f=0.26$ and $m_0=0.53$ obtained from fits to the specific heat are in serious disagreement with the measured susceptibility. It appears as if the specific heat is more sensitive to the difference between statistical and dynamical quasiparticle energies than the static susceptibility.

VI. DISCUSSION

In this paper, we have evaluated the density and spin-dependent dynamic structure factors $S_c(Q,\omega)$ and $S_I(Q,\omega)$, the static magnetic susceptibility $\chi(T)$, and the specific heat $C_V(T)$ of normal liquid ^{3}He. All these properties depend on the effective mass m^* of the quasiparticles. We have introduced a simple model (Sec. II) in which $m^*(k,\epsilon_k)=m^*(k)$ peaks to a value $m^*=2.8$ at the Fermi energy, $\epsilon_k=\epsilon_F$, and reduces to a lower mass m_0 away from ϵ_F. The model has two parameters f and m_0. The parameter f determines the energy range over which m^* drops from 2.8 to m_0. The model may be viewed as Landau theory modified to allow m^* to decrease as we move off the Fermi surface. Here, we will discuss how different properties of liquid ^{3}He depend upon m^*, and in particular how the temperature dependence of the calculated $S_I(Q,\omega)$ and $S_c(Q,\omega)$ compares with new neutron-scattering measurements (Secs. III–IV) of the total dynamic structure factor $S(Q,\omega)$.

Broadly, the Q, ω, and T dependence of $S_I(Q,\omega)$ and $S_c(Q,\omega)$ for $Q\lesssim 1$ Å^{-1} and the T dependence of $\chi(T)$ can be well described by the model with similar and consistent values of the parameters f and m_0. In our preliminary study,[31] we selected the values $m_0=1.7$ and $f=0.35$ to best reproduce the Q and ω dependence of $S_c(Q,\omega)$ and $S_I(Q,\omega)$ observed in earlier neutron-scattering measurements at $T=0.1$ K.[27,28] The present study focuses on the temperature dependence. It shows that the same model with identical parameter values predicts the temperature dependence of both $S_c(Q,\omega)$ and $S_I(Q,\omega)$ well, especially $S_I(Q,\omega)$. It is difficult to believe that this is an accident since constant-mass models such as the Landau model ($m^*=2.8$) and the paramagnon model ($m^*=1$) predict line shapes that are well outside observed uncertainty at $T=1.4$ K. Also, there are large, competing effects in the temperature dependence that cancel well in the present model to produce the correct total temperature dependence. The peaking of m^* near ϵ_F appears therefore to be an important physical feature to include in calculations of these quantities. It is unlikely that simply adding two parameters to a constant m^* model such as the Landau or paramagnon theory would bring such a marked improvement in agreement with experiment unless the model incorporated an important physical effect. We will now discuss the sensitivity of these results to the parameters f and m_0, followed by a discussion of the specific heat, which can also be well described by the model but with a much lower value of m_0.

$S_I(Q,\omega)$ and $\chi(T)$ are dominated by the low-energy ($\omega\sim 0.1$ meV) paramagnon resonance. The quasiparticles involved have therefore energies close to the Fermi energy, and the effective mass involved is $m^*(k)$ near k_F. Any combination of f and m_0 that gives a drop in $m^*(k)$ around k_F approximately as shown in Fig. 1 will give similar $S_I(Q,\omega)$ and χ. The value of m_0 alone, which sets m^* far away from k_F, is not critically important, as these quasiparticles contribute little to $S_I(Q,\omega)$ and χ.

$S_c(Q,\omega)$ is dominated by the high-energy ($\omega\sim 0.7$ meV) zero-sound mode (ZSM) and the quasiparticles involved are characterized by the effective mass $m^*(k)$ far away from k_F. Thus the ZSM energy depends on m_0 and we find that the energy is better for $m_0=1.7$ than for 1.0, i.e., for a larger effective mass. Also, an $m_0>1$ is needed to have the ZSM lie well above the particle-hole band; otherwise the zero-sound mode would be destroyed by Landau damping for $Q\gtrsim 0.6$ Å^{-1}.

The remaining discrepancies between the model and the observed temperature dependence can probably be attributed to a small weakening or reduction in the Landau parameters with increasing T which is not included in the model. Since both the paramagnon resonance and the zero-sound mode broaden with increasing temperature and the Landau param-

eters are largely determined by interactions induced via these excitations, we do expect the Landau parameters to be smaller in magnitude at $T=1.4$ K than at $T=0.1$ K. For example, there is a softening of the paramagnon resonance between $T=0.1$ and 1.4 K; i.e., at $T=1.4$ K the resonance is broader and the peak height (for $Q \geq 0.5$ Å^{-1}) is lower. This softening is largely but not fully captured in the model. It could be more fully reproduced if m^* and/or F_0^a decreased in magnitude with increasing temperature. The model also predicts a zero-sound-mode energy at $T=1.4$ K that lies somewhat above the observed value. This energy would be reduced to the observed value if F_0^s was smaller at $T=1.4$ K.

The specific heat we have evaluated is simply that of independent, noninteracting quasiparticles having energies $\epsilon(k)$ given by Eq. (9) and infinite lifetime. At low T only quasiparticles near ϵ_F, with mass $m^*=2.8$, are excited, and C_V is proportional to m^*T [cf. Eq. (14)]. From Fig. 10 we see that this C_V with a constant m^* remains very roughly proportional to T up to $T \simeq 0.5$ K [the smooth change in slope above this temperature is due to the T dependence of the chemical potential $\mu(T)$]. To reproduce the observed change in slope of C_V at $T \simeq 0.25$ K, within the present picture, we must essentially reduce m^* from $m^*=2.8$ to some much lower value m_0 at $T \simeq 0.25$ K. We can reproduce the observed value of the slope at higher temperatures if we choose $m_0=0.54$. A smaller value of f is also needed so that the change in slope occurs at $T \simeq 0.25$ K. These are the essential features of $C_V(T)$ found here, by Fantoni *et al.*,[24] and by Brown *et al.*[16] The value of $m_0=0.53$ needed to reproduce the observed $C_V(T)$ is not consistent with the $m_0 \sim 1.7$ needed in $S_c(Q,\omega)$. We will now discuss several limitations to the present calculation of $C_V(T)$.

First, the ''dynamical'' energies $\epsilon(k)$ appearing in $S(Q,\omega)$ are not the same as the ''statistical'' energies to be used in thermodynamic properties[21–23] such as $C_V(T)$. Thus an $\epsilon(k)$ which describes $S(Q,\omega)$ well need not necessarily describe $C_V(T)$ well. However, it is interesting that $\chi(T)$ does not show a pronounced change in slope at $T=0.25$ K as does $C_V(T)$. This suggests that the large and abrupt change in slope of $C_V(T)$ is specific to $C_V(T)$ and not a feature of a ''statistical'' $\epsilon(k)$ that would translate generally into all thermodynamic properties. Second, we have assumed that $\epsilon(k)$ is independent of temperature. However, as noted, the observed spin-fluctuation resonance in $S_I(Q,\omega)$ definitely broadens with increasing T. This is expected to reduce m^* at k_F. This reduction in m^* would definitely reduce the slope of $C_V(T)$ as T increases. This feature has not been included in any calculations of $C_V(T)$ to date. Third, the representation of liquid ^{3}He as a gas of independent quasiparticles, valid at $T=0$ K, may simply be unrealistic at $T \simeq 0.3$ K. The quasiparticles that are 0.3 K away from ϵ_F may be broadened and poorly defined, and the abrupt change in slope of C_V may reflect a break down of the quasiparticle picture. This breakdown may have a great impact on C_V but a much smaller impact on $S(Q,\omega)$ and $\chi(T)$. In $S(Q,\omega)$, as Q increases, the transition is from a quasiparticle picture at low Q to a particle picture at high Q. At intermediate Q an ''effective'' particle picture may be a reasonable basis. These important issues remain to be explored.

Finally, a more consistent theory in which m^* and the Landau parameters, or equivalent interactions, are calculated microscopically or in a microscopic formalism using the observed spin density $S_I(Q,\omega)$ and density $S_c(Q,\omega)$ would be an interesting next step. The resulting m^* and interactions could be used to calculate $S_I(Q,\omega)$ and $S_c(Q,\omega)$ and iterated until consistent. In this way we could determine whether an m^* that peaks near k_F emerges naturally and how well the temperature dependence of all properties is predicted.

ACKNOWLEDGMENTS

This work was supported in part by the National Science Foundation through Grant Nos. INT-9314661 and DMR-9623961. We acknowledge the Institut Laue-Langevin, Grenoble, France, for providing the neutron research facilities, and R. Chung and H. Schober for assisting the experiment.

APPENDIX

Assuming Poisson statistics, the error for N equivalent data sets (''runs'') is

$$\sigma_{set}^2=\frac{1}{N_{eff}-1}\sum_{n=1}^{N}\frac{M_n}{M}\left(\frac{I_n}{M_n}-\frac{I}{M}\right)^2, \tag{A1}$$

where $M=\Sigma_n M_n$ and $I=\Sigma_n I_n$ are the total number of monitor and detector counts, respectively, and

$$N_{eff}=\frac{\left(\sum_n M_n\right)^2}{\sum_n M_n^2}. \tag{A2}$$

Equation (A1) is identical to that employed in Ref. 42 if N_{eff} is replaced by N. N_{eff} should be used if the monitor counts M_n are not equal. If the same data are collected in a single run, the statistical error would be $\sigma_{sum}^2=I/M^2$. One expects that the ratio $R=\sigma_{set}/\sigma_{sum} \sim 1$ if the different data sets are compatible. Plotting R as a function of detector and time channel allows a rapid evaluation of any inconsistencies of the data sets, which could arise from, e.g., variations in time of the detector efficiencies or the background.

[1] G. E. Brown, J. H. Gunn, and P. Gould, Nucl. Phys. **46**, 598 (1963).
[2] C. Mahaux, P. F. Bortignon, R. A. Broglia, and C. H. Dasso, Phys. Rep. **120**, 1 (1985).
[3] J. Jeukenne, A. Lejeune, and C. Mahaux, Phys. Rep., Phys. Lett. **25C**, 83 (1975).
[4] C. Mahaux, in *Microscopic Optical Potentials*, edited by H. V. Von Geramb (Springer-Verlag, Berlin, 1979), p. 1.
[5] P. Nozières, *Theory of Interacting Fermi Systems* (Benjamin, New York, 1964).
[6] G. Baym and C. J. Pethick, in *The Physics of Liquid and Solid Helium*, edited by K. H. Bennemann and J. B. Ketterson (Wiley, New York, 1978), Pt. II, p. 1.
[7] E. Krotscheck, Phys. Rev. A **26**, 3536 (1982).
[8] B. L. Friman and E. Krotscheck, Phys. Lett. **49**, 1705 (1982).
[9] H. R. Glyde and S. I. Hernardi, Phys. Rev. B **28**, 141 (1983).
[10] H. R. Glyde and S. I. Hernardi, in *Quantum Fluids and Solids*, edited by E. D. Adams and G. G. Ihas, AIP Conf. Proc. No. 103 (AIP, New York, 1983), p. 171.
[11] B. E. Clements, C. W. Greeff, and H. R. Glyde, Phys. Rev. B **44**, 5216 (1991).
[12] B. E. Clements, C. W. Greeff, and H. R. Glyde, Phys. Rev. B **44**, 10 239 (1991).
[13] C. W. Greeff, B. E. Clements, E. F. Talbot, and H. R. Glyde, Phys. Rev. B **43**, 7595 (1991).
[14] W. F. Brinkman and S. Engelsberg, Phys. Rev. **169**, 417 (1968).
[15] G. E. Brown, *Many-Body Problems* (North-Holland, Amsterdam, 1972).
[16] G. E. Brown, C. J. Pethick, and A. Zaringhalam, J. Low Temp. Phys. **48**, 349 (1982).
[17] S. Doniach and S. Engelsberg, Phys. Rev. Lett. **17**, 750 (1966).
[18] N. F. Berk and J. R. Schrieffer, Phys. Rev. Lett. **17**, 433 (1966).
[19] D. S. Greywall, Phys. Rev. B **27**, 2747 (1983).
[20] For the Landau parameters, we use Table VII in Ref. 19, rescaled by the new values of the effective mass from D. S. Greywall, Phys. Rev. B **33**, 7520 (1986).
[21] C. J. Pethick and G. M. Carneiro, Phys. Rev. A **7**, 304 (1973).
[22] G. M. Carneiro and C. J. Pethick, Phys. Rev. B **11**, 1106 (1975).
[23] R. Balian and C. De Dominicis, Ann. Phys. (N.Y.) **62**, 229 (1971).
[24] S. Fantoni, V. R. Pandharipande, and K. E. Schmidt, Phys. Rev. Lett. **48**, 878 (1982).
[25] H. R. Glyde, *Excitations in Liquid and Solid Helium* (Oxford University Press, Oxford, 1994).
[26] K. Sköld and C. A. Pelizzari, Philos. Trans. R. Soc. London, Ser. B **290**, 605 (1980).
[27] R. Scherm, K. Guckelsberger, B. Fåk, K. Sköld, A. J. Dianoux, H. Godfrin, and W. G. Stirling, Phys. Rev. Lett. **59**, 217 (1987).
[28] B. Fåk, K. Guckelsberger, R. Scherm, and A. Stunault, J. Low Temp. Phys. **97**, 445 (1994).
[29] N. H. van Dijk, B. Fåk, K. Guckelsberger, H. Godfrin, R. Scherm, and H. Schober, Physica B **241-243**, 950 (1998).
[30] B. Fåk, N. H. van Dijk, K. Guckelsberger, H. Godfrin, R. Scherm, and H. Schober, J. Low Temp. Phys. **110**, 417 (1998).
[31] B. Fåak and H. R. Glyde, Phys. Rev. B **55**, 5651 (1997).
[32] C. H. Aldrich and D. Pines, J. Low Temp. Phys. **32**, 689 (1978); D. W. Hess and D. Pines, *ibid.* **72**, 247 (1988).
[33] H. R. Glyde and F. C. Khanna, Can. J. Phys. **55**, 1906 (1977).
[34] H. R. Glyde and F. C. Khanna, Can. J. Phys. **58**, 343 (1980).
[35] M. T. Béal-Monod, J. Low Temp. Phys. **37**, 123 (1979); **39**, 231 (1980).
[36] S. Lovesey, *Theory of Neutron Scattering from Condensed Matter* (Clarendon Press, Oxford, 1984), Vol. 1.
[37] D. L. Price and K. Sköld, in *Neutron Scattering*, Vol. 23A of *Methods of Experimental Physics*, edited by K. Sköld and D. L. Price (Academic Press, New York 1986), p. 1.
[38] A. B. Migdal, Zh. Eksp. Teor. Fiz. **34**, 1438 (1958) [Sov. Phys. JETP **7**, 996 (1958)].
[39] S. Babu and G. E. Brown, Ann. Phys. (N.Y.) **78**, 1 (1973).
[40] E. Krotscheck, J. W. Clark, and A. D. Jackson, Phys. Rev. B **28**, 5088 (1983), and references therein.
[41] W. H. Dickhoff, H. Müther, and A. Polls, Phys. Rev. B **36**, 5138 (1987).
[42] A. Stunault, K. H. Andersen, Y. Blanc, B. Fåk, H. Godfrin, K. Guckelsberger, and R. Scherm, Physica B **180-181**, 926 (1992).
[43] K. H. Andersen, Ph.D. thesis, University of Keele, 1991.
[44] A. Holas and K. S. Singwi, Phys. Rev. B **40**, 167 (1989).
[45] K. Stierstorfer, Ph.D. thesis, University of Erlangen-Nürnberg, 1991; K. Stierstorfer, C. Toepffer, and P. G. Reinhard, Phys. Lett. A **188**, 73 (1994).
[46] G. E. Brown and M. Rho, Nucl. Phys. A **372**, 397 (1981).
[47] H. Ramm, P. Pedroni, J. R. Thompson, and H. Meyer, J. Low Temp. Phys. **2**, 539 (1970).
[48] M. T. Béal-Monod, S. K. Ma, and D. R. Fredkin, Phys. Rev. Lett. **20**, 929 (1968).